Complex Dynamics in Arrays of Memristor Oscillators via the Flux-Charge Method

Complex Dynamics in Arrays of Memristor Oscillators via the Flux–Charge Method

Fernando Corinto, *Senior Member, IEEE,* and Mauro Forti

***Abstract*—The key intent of the work is to analyze complex dynamics and synchronization phenomena in a one–dimensional array of N diffusively–coupled memristor–based oscillatory/chaotic circuits, i.e., each uncoupled oscillator is a $3^{\rm rd}$–order memristor–based Chua's circuit obtained by replacing the nonlinear resistor with an ideal flux–controlled memristor. It is shown that the state space $\mathbb{R}^{4N}$ in the voltage–current domain of the array can be decomposed in ∞^N $3N$–dimensional manifolds which are positively invariant for the nonlinear dynamics. Moreover, on each manifold the array obeys a different reduced–order dynamics in the flux–charge domain. These basic properties imply that two main types of bifurcations can occur, i.e., standard bifurcations on a fixed invariant manifold induced by changing the circuit parameters and bifurcations due to the variation of initial conditions and invariant manifold, but for fixed circuit parameters. The latter bifurcation phenomena are referred to as bifurcations without parameters. The reduced dynamics on invariant manifolds, and their analytic expressions, are the key tools for a comprehensive analysis of synchronization phenomena in the array of memristor–based Chua's circuits. The main results are proved via a recently introduced technique for studying memristor–based circuits in the flux–charge domain.**

***Index Terms*—Memristor, spatio–temporal patterns, nonlinear oscillatory arrays, flux–charge analysis, invariant manifolds, synchronization.**

I. Introduction

A large deal of efforts has been traditionally devoted in circuit theory to the analysis of non–stationary steady–state behaviors in networks obtained by locally coupled arrays of simple dynamic circuits (also named cells, oscillators, units, etc.) [1]. Such dynamic arrays can be thought of as a bio–inspired circuit model of complex nonlinear phenomena observable in nature with potential applications in signal processing and computing systems. Indeed, on one hand they are a mean for reproducing, analyzing and understanding spatio–temporal nonlinear phenomena displayed by spatially extended networks found in such diverse fields as electrical engineering, computer science, biology and physics. On the other hand, complex spatio–temporal dynamics including chaos are also potentially useful for developing future analogue computing systems. Recent studies have shown that chaos can play a crucial role in searching for the global solution of combinatorial optimization problems, and chaotic relaxation oscillators with memristors [2] have been used to boots efficiency and accuracy of Hopfield–like computing networks [3].

One of the most important aspects of these research endeavors includes bifurcations and synchronization phenomena [4], [5], i.e., a scenario where all the oscillators adjust their dynamic behavior so that the whole array acts in unison and spatio–temporal patterns emerge. Synchronization phenomena in one–dimensional (1D) and bi–dimensional (2D) dynamic arrays using Chua's oscillators as building block, with various types of uni–directional, bi–directional, static and dynamic diffusive interactions, have been considered and analyzed by numerical simulations and analytic tools [6]–[8]. By extension, the influence of the network topology properties and their link with complex dynamic periodic/chaotic attractors in large biological and artificial systems have been studied in details in several works [9]–[14]. All in all, arrays of periodic/chaotic memristor–based oscillators with a wide gamut of complex attractors and including synchronization phenomena may be crucial in the next generation of brain–like computing platforms. The challenge going forward is to reproduce the modulation of the synaptic weights in neural networks in order to implement various biological phenomena such as the learning process [15]. In this regards memristor devices provide an accurate and power efficient emulator of neural synapses and biological neural codes [16]–[18]. In particular, recent works have shown the use of memristors as adaptive couplings for connecting simple Chua's oscillators in a crossbar architectures that is well suited for implementation in nanotechnology [19]–[21]. On the other hand, the works [22]–[25] consider arrays of diffusively coupled Chua's oscillators where the nonlinear resistor in each oscillator is replaced by a memristor. By numerical analysis and experiments, it is demonstrated that, due to the nonlinear dynamics of memristors, such arrays are endowed with a large variety of complex spatio–temporal phenomena [26], [27]. Interestingly, several form of synchronization can be observed by modifying, not only circuit parameters and coupling strengths, but also initial conditions of dynamic elements and, especially, of memristors. Considering that locally–connected regular architectures are especially well–suited for nanoscale implementation, and that emerging dynamic phenomena due to the presence of memristor devices are observed, it is crucial to develop analytical and numerical tools to investigate complex dynamics including synchronization phenomena in bio–inspired networks of memristor–based oscillatory cells.

In this paper we consider a 1D array of N diffusively–coupled memristor oscillators, where each memristor oscillatory circuit (MOC) is obtained by replacing the nonlinear resistor of a

The support from European Cooperation in Science and Technology "COST Action IC1401" is acknowledged.

F. Corinto is with the Department of Electronics and Telecommunications, Politecnico di Torino, Torino, Italy, e–mail: (fernando.corinto@polito.it).

M. Forti is with the Department of Information Engineering and Mathematics, University of Siena, v. Roma 56 - 53100 Siena, Italy, e–mail: (forti@diism.unisi.it).

Chua's oscillator with a flux-controlled memristor.[1] The goal is to analyze the complex dynamics, bifurcations and synchronization phenomena in NMOCs by using a recently introduced method, named flux-charge analysis method (FCAM), for the study of memristor circuits in the flux-charge (φ, q)-domain. The main results obtained in this manuscript can be summarized as follows:

- it is shown that the state space in the voltage–current (v, i)–domain can be decomposed in infinitely many manifolds that are invariant for the dynamics. Moreover, it it possible to explicitly find the state equations (SEs) describing the reduced dynamics on each invariant manifold. Respect to the result reported in [28]–[30], this step is obtained via a newly developed circuit technique based on writing suitable sets of Kirchhoff laws for the NMOC in the flux–charge (φ, q)–domain;
- via the concept of invariant manifolds, it is analytically shown that for the NMOCs there coexist infinitely many different complex attractors and dynamics, and that bifurcations without parameters, i.e., bifurcations due to changes of initial conditions for a fixed set of circuit parameters, occur. Such findings make clear initial–condition dependent nonlinear phenomena experimentally observed and reported in several publications (see for instance [22], [23], [26], [27]);
- it is shown how the explicit knowledge of invariant manifolds and the reduced dynamics on each manifold make possible to exploit results available in the literature for analyzing some relevant features of the complex nonlinear dynamics in the NMOCs. The application of such theoretic results permits to choose initial conditions such that the nonlinear dynamics in the NMOCs take place on a selected manifold (namely, the "zero–manifold", see Section IV for details), and relaying on previous analytic results in [31]–[33], various types of synchronization phenomena, including in–phase and/or anti–phase synchronization of periodic/chaotic attractors are investigated.

Although the manuscript focuses on a 1D array of N diffusively–coupled memristor oscillators, all the results reported above can be extended, *mutatis mutandis*, to any network of MOCs with dynamic diffusive couplings arranged in bi– or three–dimensional structures.

II. Memristor–based Oscillatory Circuit

Let us consider the memristor oscillatory circuit (MOC) in Fig. 1, which is obtained from the well-known Chua's circuit [34], by replacing the nonlinear locally–active resistor (Chua's diode) with an ideal locally–active flux–controlled memristor M having constitutive relation $q_M(t) = f(\varphi_M(t))$, where $\varphi_M(t)$ (resp., $q_M(t)$) is the memristor flux (resp., charge) and $f : \mathbb{R} \to \mathbb{R}$ is a smooth function which will be defined later. The remaining ideal two–terminal elements C_1, C_2, L and R are assumed to be passive. Such a MOC has been considered in literature as a prototypical circuit for studying the nonlinear dynamics, bifurcations and complex oscillatory/chaotic phenomena emerging in memristor–based bioinspired networks [35]–[38].

In the remaining part of this section we briefly recall some chief properties of the dynamics of the MOC obtained in [29], [39]. Moreover, we introduce an novel circuit technique for finding invariant manifolds in a MOC, which is effective also to study the nonlinear dynamics and synchronization properties in arrays of diffusively–coupled MOCs (see Section IV). Let us:

- introduce the state variables corresponding to the four dynamic elements, i.e., C_1, C_2, L and M, in the (v, i)–domain
$$\mathbf{w}(t) = (v_{C_1}(t), v_{C_2}(t), i_L(t), \varphi_M(t))^T \in \mathbb{R}^4$$
- assume $-\infty < t_0 < +\infty$ to be a given finite instant and let $v_{C_1}(t_0)$, $v_{C_2}(t_0)$, $i_L(t_0)$, $\varphi_M(t_0)$ be the initial conditions (ICs) at t_0 for the state variables. Moreover, let $q_{C_1}(t_0) = C_1 v_{C_1}(t_0)$, $q_{C_2}(t_0) = C_2 v_{C_2}(t_0)$, $\varphi_L(t_0) = L i_L(t_0)$ and $q_M(t_0) = f(\varphi_M(t_0))$;
- define, in addition to the voltage $v(t)$ and current $i(t)$ for each two–terminal element in the MOC, the flux $\varphi(t)$, the charge $q(t)$ and also the incremental flux and charge $(t \geq t_0)$
$$\varphi(t; t_0) \;=\; \varphi(t) - \varphi(t_0) \;=\; \int_{t_0}^{t} v(\tau) d\,\tau$$
$$q(t; t_0) \;=\; q(t) - q(t_0) \;=\; \int_{t_0}^{t} i(\tau) d\,\tau$$

Given the ICs in the (v, i)–domain, FCAM [28] permits to associate the MOC in Fig. 1 with the reduced–order circuit in the (φ, q)–domain reported in Fig. 2. Each two–terminal element is represented by its equivalent circuit in the (φ, q)–domain and the circuit can be analyzed by Kirchhoff flux law (KφL) and Kirchhoff charge law (KqL) for incremental charges and fluxes. Note that the reduction of order for the associated circuit is simply due to the fact that in the (φ, q)–domain the ideal memristor results to be a memoryless nonlinear element.

By using KφLs and KqLs, the following SEs describing the MOC in the (φ, q)–domain are obtained

$$\begin{aligned} C_1 \frac{d\varphi_{C_1}(t; t_0)}{dt} =& -\frac{1}{R}(\varphi_{C_1}(t; t_0) - \varphi_{C_2}(t; t_0)) + q_{C_1}(t_0) \\ & - f(\varphi_{C_1}(t; t_0) + \varphi_M(t_0)) + f(\varphi_M(t_0)) \end{aligned} \tag{1a}$$

$$\begin{aligned} C_2 \frac{d\varphi_{C_2}(t; t_0)}{dt} =& -\frac{1}{R}(\varphi_{C_2}(t; t_0) - \varphi_{C_1}(t; t_0)) + q_{C_2}(t_0) \\ & - q_L(t; t_0) \end{aligned} \tag{1b}$$

$$L \frac{dq_L(t; t_0)}{dt} = \varphi_{C_2}(t; t_0) + \varphi_L(t_0) \tag{1c}$$

$$\begin{aligned} \varphi_{C_1}(t_0; t_0) =& 0 \\ \varphi_{C_2}(t_0; t_0) =& 0 \\ q_L(t_0; t_0) =& 0 \end{aligned}$$

for all $t \geq t_0$, where we have taken into account that $\varphi_{C_1}(t; t_0) = \varphi_M(t; t_0)$. It is apparent that (1) is an initial value

[1] We will use the acronym NMOC for the considered array of N interconnected MOCs.

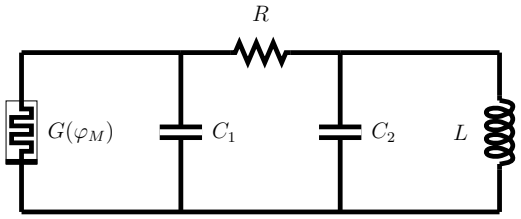

Figure 1: Memristor Oscillatory Circuit (MOC) obtained from the Chua's circuit by replacing the nonlinear locally–active resistor with an ideal locally–active flux–controlled memristor ($G(\varphi_M) = f'(\varphi_M)$).

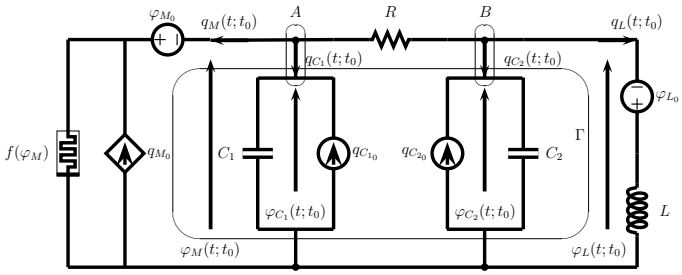

Figure 2: MOC of Fig. 1 in the (φ, q)–domain where $q_{C_{1_0}} = q_{C_1}(t_0)$, $q_{C_{2_0}} = q_{C_2}(t_0)$, $\varphi_{L_0} = \varphi_L(t_0)$ and $\varphi_{M_0} = \varphi_M(t_0)$.

problem (IVP) for a third–order system of ODEs in the three state variables $(\varphi_{C_1}(t;t_0), \varphi_{C_2}(t;t_0), q_L(t;t_0))$ in the (φ, q)–domain. Note that the right-hand side of (1) contains constant terms depending on the ICs for the state variables in the (v, i)–domain.

On the basis of FCAM [28], the time differentiation of (1) produces the SEs of the MOC in the (v, i)–domain

$$C_1 \frac{dv_{C_1}(t)}{dt} = -\frac{1}{R}(v_{C_1}(t) - v_{C_2}(t)) - f'(\varphi_M(t))v_{C_1}(t) \tag{2a}$$

$$C_2 \frac{dv_{C_2}(t)}{dt} = -\frac{1}{R}(v_{C_2}(t) - v_{C_1}(t)) - i_L(t) \tag{2b}$$

$$L \frac{di_L(t)}{dt} = v_{C_2}(t) \tag{2c}$$

$$\frac{d\varphi_M(t)}{dt} = v_{C_1}(t) \tag{2d}$$

for all $t \geq t_0$, with ICs $\mathbf{w}(t_0) = (v_{C_1}(t_0), v_{C_2}(t_0), i_L(t_0), \varphi_M(t_0))^T$ (the prime means the derivative with respect to the argument of $f(\cdot)$). Here, we noted that $\varphi_{C_1}(t;t_0) + \varphi_M(t_0) = \varphi_M(t;t_0) + \varphi_M(t_0) = \varphi_M(t)$. The SEs (2) result to be an IVP for a fourth–order system of ODEs in the state variables $\mathbf{w}(t)$.

The order reduction of the dynamics of the MOC in the (φ, q)–domain, with respect to the (v, i)–domain, can be better understood when noting that the state space in the (v, i)–domain can be decomposed in infinitely many invariant manifolds. To make clear such concept, let us consider the function $Q : \mathbb{R}^4 \to \mathbb{R}$ of the state variables in the (v, i)–domain

$$Q(\mathbf{w}) = f(\varphi_M) + \frac{1}{R}\varphi_M + C_1 v_{C_1} - \frac{L}{R} i_L \tag{3}$$

and, for any $Q_0 \in \mathbb{R}$, let

$$\mathcal{M}(Q_0) = \{\mathbf{w} \in \mathbb{R}^4 : Q(\mathbf{w}) = Q_0\}. \tag{4}$$

Note that $\mathcal{M}(Q_0)$ is a three–dimensional manifold in $\mathbb{R}^4$ that coincides with the Q_0–level set of function $Q(\cdot)$. Also note that, for any $\mathbf{w} \in \mathbb{R}^4$, we have $\mathbf{w} \in \mathcal{M}(Q(\mathbf{w}))$.

Property 1: The state space $\mathbb{R}^4$ of the MOC in the (v, i)–domain can be decomposed in ∞^1 three–dimensional manifolds $\mathcal{M}(Q_0)$ by varying $Q_0 \in \mathbb{R}$. Manifolds are nonintersecting and they span the whole state space $\mathbb{R}^4$. Each manifold is positively invariant for the dynamics of the MOC in the (v, i)–domain, i.e., if the ICs $\mathbf{w}(t_0) = (v_{C_1}(t_0), v_{C_2}(t_0), i_L(t_0), \varphi_M(t_0))^T \in \mathcal{M}(Q_0)$, where $Q_0 = Q(\mathbf{w}(t_0))$, then the solution $(v_{C_1}(t), v_{C_2}(t), i_L(t), \varphi_M(t))$ of the IVP (2) belongs to $\mathcal{M}(Q_0)$ for any $t \geq t_0$. On each manifold $\mathcal{M}(Q_0)$ the dynamics of the MOC is described in the (φ, q)-domain by the third–order system of ODEs (1).

Proof: Suppose for contradiction that there exists $\mathbf{x} \in \mathbb{R}^4$ such that $\mathbf{w} \in \mathcal{M}(Q_1) \cap \mathcal{M}(Q_2)$, with $Q_1 \neq Q_2$. This implies $Q(\mathbf{w}) = Q_1$ and $Q(\mathbf{w}) = Q_2$, which is a contradiction. This shows that the manifolds are nonintersecting. To see that they cover the whole space $\mathbb{R}^4$ it is enough to recall that, for any $\mathbf{w} \in \mathbb{R}^4$, we have $\mathbf{w} \in \mathcal{M}(Q(\mathbf{w}))$.

Let us show that each manifold is positively invariant by analyzing the associated circuit of the MOC in the (φ, q)-domain. We have from KqL at the cutset made of nodes A and B (see Fig. 2)

$$q_M(t;t_0) + q_{C_1}(t;t_0) + q_{C_2}(t;t_0) + q_L(t;t_0) = 0$$

for any $t \geq t_0$. From KqL at node B

$$q_R(t;t_0) + q_{C_2}(t;t_0) + q_L(t;t_0) = 0$$

and from KφL at the loop Γ (see again Fig. 2)

$$\varphi_M(t;t_0) = \varphi_R(t;t_0) + \varphi_L(t;t_0).$$

These two last equations yield

$$q_L(t;t_0) = \frac{\varphi_M(t;t_0) - \varphi_L(t;t_0)}{R} - q_{C_2}(t;t_0)$$

and substituting in the first equation we obtain

$$q_M(t;t_0) + q_{C_1}(t;t_0) + \frac{\varphi_M(t;t_0) - \varphi_L(t;t_0)}{R} = 0.$$

Since $q_M(t) = f(\varphi_M(t))$, we have

$$\begin{aligned} f(\varphi_M) + \frac{1}{R}\varphi_M + C_1 v_{C_1} - \frac{L}{R} i_L &= f(\varphi_M(t_0)) + \frac{1}{R}\varphi_M(t_0) \\ &+ C_1 v_{C_1}(t_0) - \frac{L}{R} i_L(t_0) \end{aligned}$$

for any $t \geq t_0$. ■

Remark 1: The technique for proving invariance of $\mathcal{M}(Q_0)$ in Property 1 is based on KφLs and KqLs of the associated circuit and, as such, it differs from that given in [29], that is instead based on algebraic manipulations of SEs in the

(φ, q)-domain. This new proof, in addition to being simpler and based on circuit theoretic ideas, has also the advantage of lending itself to an extension to arrays of coupled MOCs (cf. Property 2 in Section III). We also note that the invariance of manifold $\mathcal{M}(Q_0)$ is equivalent to saying that $Q(\cdot)$ as in (3) is an *invariant of motion* for the dynamics of the MOC in the (v, i)–domain.

A. Complex Dynamics in the single MOC

The previous section has pointed out how the dynamic behavior of the MOC in Fig. 2 takes place on invariant manifolds and on each manifold the nonlinear dynamics is described by (1). It is convenient to cast the SEs (1) in a more compact normal form. To this end, let us define the parameters (see also Table I in [29] for more details)

$$\alpha = \frac{C_1}{C_2}, \;\; \beta = \frac{R^2 C_2}{L} \tag{5}$$

introduce the normalized time $t \to t/(RC_2)$ and the change of variables

$$x(t) = \varphi_{C_1}(t; t_0) + \varphi_M(t_0) = \varphi_M(t) \tag{6a}$$
$$y(t) = \varphi_{C_2}(t; t_0) + \varphi_L(t_0) \tag{6b}$$
$$z(t) = -Rq_L(t; t_0) + \varphi_L(t_0) - \varphi_M(t_0) + Rq_{C_2}(t_0). \tag{6c}$$

The following SEs in adimensional form for $t \geq t_0$ follow

$$\frac{dx(t)}{dt} = \alpha(-x(t) + y(t) - n(x(t))) + X_0 \tag{7a}$$
$$\frac{dy(t)}{dt} = x(t) - y(t) + z(t) \tag{7b}$$
$$\frac{dz(t)}{dt} = -\beta y(t) \tag{7c}$$
$$\begin{aligned} x(t_0) &= \varphi_M(t_0) \\ y(t_0) &= \varphi_L(t_0) = Li_L(t_0) \\ z(t_0) &= \varphi_L(t_0) - \varphi_M(t_0) + Rq_{C_2}(t_0) \\ &= Li_L(t_0) - \varphi_M(t_0) + RC_2 v_{C_2}(t_0) \end{aligned} \tag{7d}$$

where $n(x(t)) = Rf(x(t))$ and

$$\begin{aligned} X_0 &= \alpha RQ(\mathbf{w}(t_0)) \\ &= \alpha(n(\varphi_M(t_0)) + \varphi_M(t_0) + RC_1 v_{C_1}(t_0) - Li_L(t_0)) \end{aligned} \tag{8a}$$

which is a term depending on the ICs for the state variables in the (v, i)–domain.

It is worth noting that, when the ICs $v_{C_1}(t_0)$, $i_L(t_0)$ and $\varphi_M(t_0)$ are such that $X_0 = 0$, i.e., $Q(\mathbf{w}(t_0)) = 0$, and the nonlinear dynamics of the MOC is on the invariant *zero–manifold* $\mathcal{M}(0)$, the SEs (7) formally coincide with those of the classical Chua's circuit [34]. It follows that MOC can undergo *standard bifurcations* on the *fixed manifold* $\mathcal{M}(0)$ by varying the circuit parameters α and β. On the other hand, due to the term X_0 at the right–hand side of (7), on each manifold $\mathcal{M}(Q_0)$ MOC exhibits a rich variety of dynamic behaviors and different coexisting attractors. The dynamic behavior of a nonlinear system (number and stability of equilibrium points and limit cycles, etc.) is indeed heavily dependent also on constant terms in the vector field [40], [41]. We can thus envisage an alternative mechanism to induce bifurcations, i.e., bifurcations due to the change of ICs for *fixed circuit parameters*. Such bifurcations are also named *bifurcations without parameters*.

Nonlinear dynamics and bifurcations in the MOCs have been also investigated in [29], [39], where, in particular, the memristor constitutive relation is chosen as

$$f(\varphi_M) = -\frac{8}{7}\varphi_M + \frac{4}{63}\varphi_M^3 \tag{9}$$

which is a good smooth approximation of the nonlinear Chua's diode characteristic [42]. An accurate characterization of the bifurcation diagram in memristor–based Chua's circuits, including the analysis of co–existing hyperchaotic attractors, is reported in [26], [27]. For the sake of completeness, and to make the manuscript self–consistent, we briefly summarize the Hopf and period–doubling bifurcations without parameters leading to a scenario where complex dynamics depending on the choice of ICs and invariant manifold is observed. In particular, some selected numerical simulations of (7) by varying Q_0 (and, hence, X_0), for suitable fixed sets of circuit parameters (L, C_1, C_2, R) are reported. Figures 3 and 5 present the simulations of (7) with the different sets of ICs $\varphi_M(t_0) \in \{0, 0.25, 0.5\}$, $q_{C_1}(t_0) = \varphi_L(t_0) = 0$, $q_{C_2}(t_0) = 1$ and the fixed parameters, $C_1 = 1$, $R = 1$, $\alpha = 9.5$ and $\beta = 15$.

It follows that:

- $Q_0 = 0$ when $\varphi_M(t_0) = 0$
- $Q_0 = -0.0347$ when $\varphi_M(t_0) = 0.25$
- $Q_0 = -0.0635$ when $\varphi_M(t_0) = 0.5$.

The projection on the (x, y)–plane of the chaotic attractor obtained for $Q_0 = 0$ (resp., $Q_0 = -0.0347$) is reported in Fig. 3 (resp., Fig. 5). The period–4 attractor obtained for $Q_0 = -0.0635$ is shown in Figure 6. Clearly, the MOC in Fig. 2 undergoes a period–doubling bifurcation with a change from the periodic attractor to the single–scroll chaotic attractor and successively to the double–scroll chaotic attractor. Lyapunov exponents associated to the double–scroll chaotic attractor for different values of X_0 are shown in Fig. 4.

It is apparent that such bifurcations are induced by changing the ICs (i.e., the constant Q_0) whereas the circuit parameters (L, C_1, C_2, R) are not varied, i.e., we are dealing with a bifurcation without parameters scenario with coexistence of different attractors for the same set of parameters.

III. One–dimensional Arrays of MOCs

Numerous biological and physical systems are described as a collection of interacting cells (e.g., neurons, oscillators, etc.) and the emergence of a common complex dynamical behavior, which might differ significantly from those of each individual subsystem, is due to the interaction effects. Synchronization phenomena represent one of the chief aspect of dynamical processes in non–trivial complex network topologies. Roughly speaking, synchronization can be considered as the "adjustment of rhythms of self–sustained periodic/chaotic oscillators due to their weak interaction (coupling)" and it is considered one of the best way to explore the collective behavior of networks.

In order to study synchronization phenomena in a 1D array of N diffusively–coupled identical MOCs (hereinafter denoted

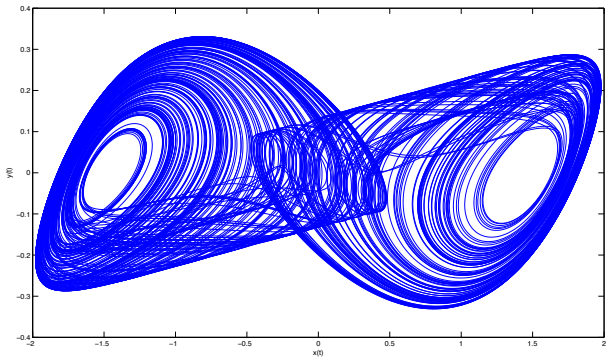

Figure 3: Double–scroll chaotic attractor of the third–order memristor–based oscillator in Fig. 2 with $Q_0 = 0$. The ICs and the circuit parameters are given in the text.

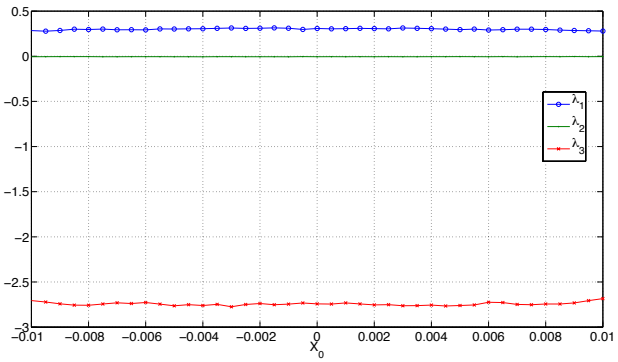

Figure 4: Lyapunov exponents as function of X_0 in the third–order memristor–based oscillator in Fig. 2. The ICs and the circuit parameters are given in the text.

by NMOCs, for short), we consider their description in the flux–charge domain given by the following SEs

$$\begin{aligned} C_1\frac{d\varphi_{C_{1,i}}(t;t_0)}{dt} &= -\frac{1}{R}(\varphi_{C_{1,i}}(t;t_0)-\varphi_{C_{2,i}}(t;t_0)) \\ &\quad - f(\varphi_{C_{1,i}}(t;t_0)+\varphi_{M_{0,i}})+f(\varphi_{M_{0,i}})+q_{C_{1,i}}(t_0) \\ &\quad + \sum_{k\in\mathcal{N}_i}\frac{1}{R_{ik}}(\varphi_{C_{1,k}}(t;t_0)-\varphi_{C_{1,i}}(t;t_0)) \end{aligned} \tag{10a}$$

$$\begin{aligned} C_2\frac{d\varphi_{C_{2,i}}(t;t_0)}{dt} &= -\frac{1}{R}(\varphi_{C_{2,i}}(t;t_0)-\varphi_{C_{1,i}}(t;t_0)) \\ &\quad - q_{L,i}(t;t_0)+q_{C_{2,i}}(t_0) \end{aligned} \tag{10b}$$

$$L\frac{dq_{L,i}(t;t_0)}{dt} = \varphi_{C_{2,i}}(t;t_0)+\varphi_{L,i}(t_0) \tag{10c}$$

$$\begin{aligned} \varphi_{C_{1,i}}(t_0;t_0) &= 0 \\ \varphi_{C_{2,i}}(t_0;t_0) &= 0 \\ q_{L,i}(t_0;t_0) &= 0 \end{aligned}$$

where $i = 1,\ldots,N$ identifies the i^{th} MOC, whereas k assumes values in the set $\mathcal{N}_i = \{i-r,\ldots,i,\ldots,i+r\}$ and specifies the $2r+1$ ($r \geq 1$) MOCs in the neighbor the i^{th} MOC and connected to it. Let us denote by R_{ik} the resistor connecting the i^{th} and k^{th} MOCs through $\varphi_{C_{1,i}}(t;t_0)$ and $\varphi_{C_{1,k}}(t;t_0)$. Hereinafter, we also suppose that the boundary conditions be

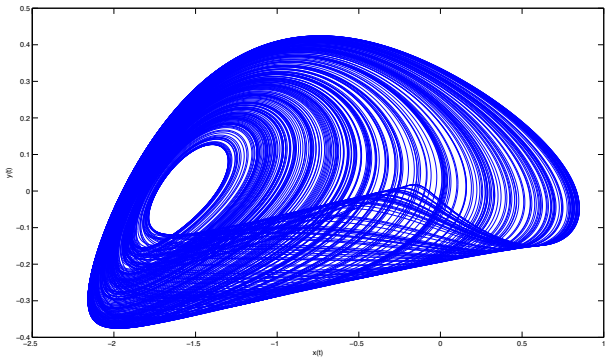

Figure 5: Single–scroll chaotic attractor of the third–order memristor–based oscillator in Fig. 2 with $Q_0 = -0.0347$. The ICs and the circuit parameters are given in the text.

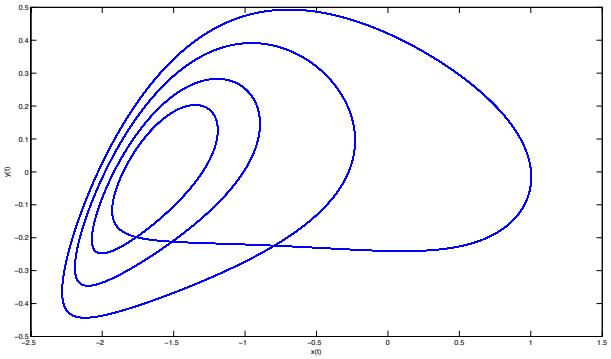

Figure 6: Periodic attractor of the third–order memristor–based oscillator in Fig. 2 with $Q_0 = -0.0635$. The ICs and the circuit parameters are given in the text.

of Dirichlet type (i.e., $\varphi_{C_{1,0}}(t;t_0) = \varphi_{C_{1,N+1}}(t;t_0) = 0$). Such SEs define an IVP for a system of $3N$ coupled first-order ODEs. The structure of the NMOC is reported in Fig. 7.

The SEs in the (v,i)–domain of the the NMOCs are readily obtained by time differentiation of (10)

$$\begin{aligned} C_1\frac{dv_{C_{1,i}}(t)}{dt} &= -\frac{1}{R}(v_{C_{1,i}}(t)-v_{C_{2,i}}(t)) - f'(\varphi_{M,i}(t))v_{C_{1,i}}(t) \\ &\quad + \sum_{k\in\mathcal{N}_i}\frac{1}{R_{ik}}(v_{C_{1,k}}(t)-v_{C_{1,i}}(t)) \end{aligned} \tag{11a}$$

$$C_2\frac{dv_{C_{2,i}}(t)}{dt} = -\frac{1}{R}(v_{C_{2,i}}(t)-v_{C_{1,i}}(t)) - i_{L,i}(t) \tag{11b}$$

$$L\frac{di_{L,i}(t)}{dt} = v_{C_{2,i}}(t) \tag{11c}$$

$$\frac{d\varphi_{M,i}(t)}{dt} = v_{C_{1,i}}(t) \tag{11d}$$

$$\begin{aligned} v_{C_{1,i}}(t_0) &= v_{C_{1,i}}(t_0) \\ v_{C_{2,i}}(t_0) &= v_{C_{2,i}}(t_0) \\ i_{L,i}(t_0) &= i_{L,i}(t_0) \\ \varphi_{M,i}(t_0) &= \varphi_{M,i}(t_0). \end{aligned}$$

The SEs in the (v,i)–domain are an IVP for a system of $4N$ coupled first–order ODEs in the state variables

$$\begin{aligned} \mathbf{w}_c(t) \;=\; & (v_{C_{1,1}}, v_{C_{2,1}}, i_{L,1}, \varphi_{M,1}, \\ & \ldots, v_{C_{1,N}}, v_{C_{2,N}}, i_{L,N}, \varphi_{M,N})^T \in \mathbb{R}^{4N}. \end{aligned}$$

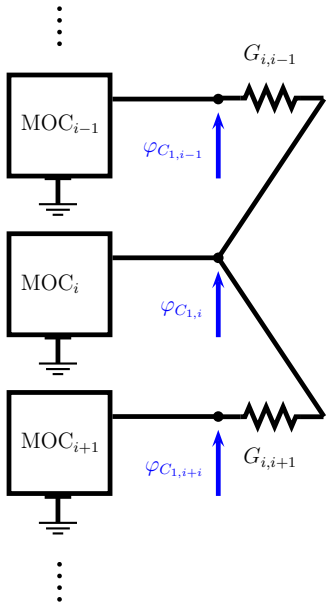

Figure 7: One–dimensional array of N diffusively–coupled identical MOCs.

Most importantly, manifolds in the state space $\mathbb{R}^{4N}$ in the (v,i)-domain of (11) can be identified. To this end, let us define functions $Q_i : \mathbb{R}^{4N} \to \mathbb{R}$, $i = 1, 2, \ldots, N$, as follows

$$\begin{aligned} Q_i(\mathbf{w}_c) &= f(\varphi_{M,i}) + \frac{1}{R}\varphi_{M,i} + C_1 v_{C_{1,i}} - \frac{L}{R} i_{L,i} \\ &- \sum_{k\in\mathcal{N}_i} \frac{1}{R_{ik}}(\varphi_{M,k} - \varphi_{M,i}). \end{aligned} \tag{12}$$

For any $\mathbf{Q}_0 = (Q_{0,1}, \ldots, Q_{0,N})^T \in \mathbb{R}^N$, let

$$\mathcal{M}_c(\mathbf{Q}_0) = \{\mathbf{w}_c \in \mathbb{R}^{4N} : Q_i(\mathbf{w}_c) = Q_{0,i}, i = 1, 2, \ldots, N\}.$$

Note that $\mathcal{M}_c(\mathbf{Q}_0)$ is a $3N$–dimensional manifold in $\mathbb{R}^{4N}$ that coincides with the $\mathbf{Q}_0$–level set of function $\mathbf{Q}(\cdot) = (Q_1(\cdot), Q_2(\cdot), \ldots, Q_n(\cdot))^T$.

Property 2: The state space $\mathbb{R}^{4N}$ of the NMOCs in the (v,i)–domain can be decomposed in ∞^N $3N$-dimensional manifolds $\mathcal{M}_c(\mathbf{Q}_0)$ by varying $\mathbf{Q}_0 \in \mathbb{R}^N$. Manifolds are nonintersecting and they span the whole state space $\mathbb{R}^{4N}$. Each manifold is positively invariant for the dynamics of NMOC in the (v,i)-domain, i.e., if the ICs $\mathbf{w}(t_0) \in \mathcal{M}_c(\mathbf{Q}_0)$, where $\mathbf{Q}_0 = \mathbf{Q}(\mathbf{w}_c(t_0))$, then the solution of the IVP (11) belongs to $\mathcal{M}_c(\mathbf{Q}_0)$ for any $t \geq t_0$. On each manifold $\mathcal{M}_c(\mathbf{Q}_0)$ the dynamics of the MOC is described in the (φ, q)-domain by the system of ODEs (10), whose order is $3N$.

Proof: The first part of the proof is analogous to that of Property 1 and is omitted for brevity. Let us show that each manifold is positively invariant. We have from KqL at the cutset with nodes A, B and R_{ik}, $k \in \mathcal{N}_i$, of the i^{th} MOC

$$\begin{aligned} &q_{M,i}(t;t_0) + q_{C_{1,i}}(t;t_0) + q_{C_{2,i}}(t;t_0) + q_{L,i}(t;t_0) \\ &- \sum_{k\in\mathcal{N}_i} \frac{1}{R_{ik}}(\varphi_{M,k}(t;t_0) - \varphi_{M,i}(t;t_0)) = 0 \end{aligned}$$

for any $t \geq t_0$. Arguing as in the proof of Property 1, KqL at node B and KφL at loop Γ of the i^{th} MOC yield

$$q_{L,i}(t;t_0) = \frac{\varphi_{M,i}(t;t_0) - \varphi_{L,i}(t;t_0)}{R} - q_{C_{2,i}}(t;t_0)$$

and substituting in the first equation we obtain

$$\begin{aligned} &q_{M,i}(t;t_0) + q_{C_{1,i}}(t;t_0) + \frac{\varphi_{M,i}(t;t_0) - \varphi_{L,i}(t;t_0)}{R} \\ &- \sum_{k\in\mathcal{N}_i} \frac{1}{R_{ik}}(\varphi_{M,k}(t;t_0) - \varphi_{M,i}(t;t_0)) = 0. \end{aligned}$$

Then we have

$$\begin{aligned} &f(\varphi_{M,i}(t)) + \frac{1}{R}\varphi_{M,i}(t) + C_1 v_{C_{1,i}}(t) \\ &-\frac{L}{R} i_{L,i}(t) + \sum_{k\in\mathcal{N}_i} \frac{1}{R_{ik}}(\varphi_{M,k}(t) - \varphi_{M,i}(t)) \\ &= f(\varphi_{M,i}(t_0)) + \frac{1}{R}\varphi_{M,i}(t_0) + C_1 v_{C_{1,i}}(t_0) \\ &-\frac{L}{R} i_{L,i}(t_0) - \sum_{k\in\mathcal{N}_i} \frac{1}{R_{ik}}(\varphi_{M_{0,k}} - \varphi_{M_{0,i}}) \end{aligned}$$

for any $t \geq t_0$ and $i = 1, 2, \ldots, N$. ■

Remark 2: Note that $Q_i(\mathbf{w}_c)$ $(i = 1, 2, \ldots, N)$ provide N invariants of motion for the dynamics of the NMOCs in the (v,i)–domain.

A. Adimensional Normal Form of SEs in the (φ, q)-domain

Using the parameters in (5) and the change of variables in (6) for each MOC, the adimensional SEs of the whole NMOCs result to be (for all $i = 1, \ldots, N$)

$$\begin{aligned} \frac{dx_i(t)}{dt} &= \alpha(-x_i(t) + y_i(t) - n(x_i(t))) + X_{0,i} \\ &+ \Big(\sum_{k\in\mathcal{N}_i} d_{ik}(x_k(t) - x_i(t)) \\ &- \sum_{k\in\mathcal{N}_i} d_{ik}(\varphi_{M,k}(t_0) - \varphi_{M,i}(t_0)) \Big) \end{aligned} \tag{13a}$$

$$\frac{dy_i(t)}{dt} = x_i(t) - y_i(t) + z_i(t) \tag{13b}$$

$$\frac{dz_i(t)}{dt} = -\beta y_i(t) \tag{13c}$$

$$\begin{aligned} x_i(t_0) &= \varphi_{M,i}(t_0) \\ y_i(t_0) &= \varphi_{L,i}(t_0) = L i_{L,i}(t_0) \\ z_i(t_0) &= \varphi_{L,i}(t_0) - \varphi_{M,i}(t_0) + R q_{C_{2,i}}(t_0) \\ &= L i_{L,i}(t_0) - \varphi_{M,i}(t_0) + RC_2 v_{C_{2,i}}(t_0) \end{aligned} \tag{13d}$$

where $d_{ik} = \alpha R / R_{ik}$ and

$$\begin{aligned} X_{0,i} &= \alpha RQ(v_{C_{1,i}}(t_0), v_{C_{2,i}}(t_0), i_{L,i}(t_0), \varphi_{M,i}(t_0)) \\ &= \alpha(n(\varphi_{M,i}(t_0)) + \varphi_{M,i}(t_0) + RC_1 v_{C_{1,i}}(t_0) \\ &- L i_{L,i}(t_0)) \end{aligned} \tag{14}$$

with $Q(\cdot)$ is as in (3). Introducing the parameters

$$X_{c_{0,i}} = X_{0,i} - \sum_{k\in\mathcal{N}_i} d_{ik}(\varphi_{M,k}(t_0) - \varphi_{M,i}(t_0)) \tag{15}$$

the SEs (13) can be written in the form (when $r = 1$ and $\mathcal{N}_i = \{i-1, i, i+1\}$, then)

$$\frac{dx_i(t)}{dt} = \alpha(-x_i(t) + y_i(t) - n(x_i(t))) + \sum_{k\in\mathcal{N}_i} d_{ik}\left(x_k(t) - x_i(t)\right) + X_{c_{0,i}} \tag{16a}$$

$$\frac{dy_i(t)}{dt} = x_i(t) - y_i(t) + z_i(t) \tag{16b}$$

$$\frac{dz_i(t)}{dt} = -\beta y_i(t). \tag{16c}$$

This shows that the NMOCs result to be analogous to an array of diffusively coupled Chua's circuits. A relevant difference is however due to the additional constants terms $X_{c_{0,i}}$ at the right–hand side of (16), depending on the ICs for the state variables in the (v, i)–domain, which need to be carefully taken into account in the investigation of synchronization phenomena.

IV. Synchronization Phenomena in the NMOCs

The analytical results on invariant manifolds for the single MOC and the whole NMOCs are instrumental in analyzing synchronization phenomena and in exploiting the theory of weakly–connected oscillatory networks [43]. In particular, in order to demonstrate the role of invariant manifolds on the occurrence of synchronization in the NMOCs, let us introduce the synchronization manifold of the whole NMOCs in the (φ, q)–domain

$$\begin{aligned}\mathcal{M}_S \;=\; & \{(x_1, y_1, z_1, \ldots, x_N, y_N, z_N) \in \mathbb{R}^{3N} : \\ & x_1 = \cdots = x_N; \\ & y_1 = \cdots = y_N; \\ & z_1 = \cdots = z_N\} \subset \mathbb{R}^{3N}\end{aligned}$$

and define the synchronization errors

$$\mathbf{e}_{ij} = \begin{pmatrix} x_i - x_j \\ y_i - y_j \\ z_i - z_j \end{pmatrix}$$

for $i, j = 1, 2 \ldots, N$. The manifold $\mathcal{M}_S$ is positively invariant for the dynamics of (16) if and only if $\mathbf{w}_c(t) \in \mathcal{M}_S$ implies $d\,\mathbf{e}_{ij}(t)/dt = 0$, $t \geq t_0$. Since for $\mathbf{w}_c(t) \in \mathcal{M}_S$

$$\frac{d\,\mathbf{e}_{ij}(t)}{dt} = \begin{pmatrix} X_{c_{0,i}} - X_{c_{0,j}} \\ 0 \\ 0 \end{pmatrix}$$

then $\mathcal{M}_S$ is positively invariant for the dynamics of (16) if and only if

$$X_{c_{0,i}} = X_{c_0} \tag{17}$$

for any $i = 1, 2, \ldots, N$, and means that the uncoupled MOCs are identical (same set of equations (7)). Note that (17) is equivalent to

$$X_{0,i} - \sum_{k\in\mathcal{N}_i} d_{ik}(\varphi_{M,k}(t_0) - \varphi_{M,i}(t_0)) = X_{c_0} \tag{18}$$

for any $i = 1, 2, \ldots, N$.

If the NMOCs reach the state of complete synchronization (CS), that is

$$\lim_{t\to+\infty} \mathbf{e}_{ij}(t) = 0$$

for any $i, j = 1, 2, \ldots, N$, it can be seen that $\forall i = 1, 2, \ldots, N$

$$\lim_{t\to+\infty} Q(v_{C_{1,i}}(t), v_{C_{2,i}}(t), i_{L,i}(t), \varphi_{M,i}(t)) = \frac{X_{c_0}}{\alpha R}.$$

In other words, under the condition of CS each uncoupled MOC asymptotically evolves on the same manifold defined by

$$\begin{pmatrix} x_i(t) \\ y_i(t) \\ z_i(t) \end{pmatrix} \to \mathcal{M}\left(\frac{X_{c_0}}{\alpha R}\right) \tag{19}$$

as $t \to +\infty$, for any $i = 1, 2, \ldots, N$, where $\mathcal{M}(\cdot)$ is as in (4).

A sketch of the proof of this result is obtained considering that $Q_i(\cdot)$ as in (12) are invariants of motion for NMOCs in the (v, i)–domain (cf. Property 2), hence

$$\alpha R Q_i(\mathbf{w}_c(t)) = \alpha R Q_i(\mathbf{w}_c(t_0)) = X_{c_0}$$

for any $t \geq t_0$ and $i = 1, \ldots, N$. Then, (12) implies

$$\begin{aligned}\alpha R\Big[& Q(v_{C_{1,i}}(t), v_{C_{2,i}}(t), i_{L,i}(t), \varphi_{M,i}(t)) \\ & - \sum_{k\in\mathcal{N}_i} \frac{1}{R_{ik}}(\varphi_{M,k}(t) - \varphi_{M,i}(t))\Big] \;=\; X_{c_0}\end{aligned}$$

for $t \geq t_0$. The result follows by taking the limit as $t \to +\infty$ in the previous expression and considering that $x_i(t) = \varphi_{M,i}(t)$ and that in the case of CS we have $\sum_{k\in\mathcal{N}_i} d_{ik}(\varphi_{M,k}(t) - \varphi_{M,i}(t)) \to 0$ as $t \to +\infty$.

Remark 3: Since $x_i(t) = \varphi_M(t)$, it can be immediately checked that, in the case of CS of (16) in the (φ, q)–domain, the state variables $\mathbf{w}_c(t)$ in the (v, i)–domain also achieve CS.

A. Numerical Simulations

This section reports numerical simulations of 1D arrays with $N = 4$ identical MOCs. For the sake of simplicity, and following the analysis in the previous sections, let us assume *homogeneous ICs on the fluxes of memristors* (i.e., $\varphi_{M,i}(t_0) = \varphi_0$) and $v_{C_{1,i}}(t_0) = i_{L,i}(t_0)) = 0$ for all $i = 1, \ldots, N$. It follows that condition (18) is satisfied and reduces to (see also (14))

$$X_{c_0} = X_{0,i} = \alpha(n(\varphi_0) + \varphi_0) \tag{20}$$

for $i = 1, \ldots, 4$. In addition, it is assumed that φ_0 is such that $X_{c_0} = 0$, that is, the values $\varphi_0 \in \{-1.5, 0, 1.5\}$ are derived by using the expression (9). Under such assumptions, each uncoupled MOC evolves on the zero–manifold $\mathcal{M}(0)$ on which its nonlinear dynamics is the same of the classical Chua's circuit.

The evolution of NMOCs is described by (16) with ICs

$$x_i(t_0) = \varphi_0 \tag{21a}$$

$$y_i(t_0) = 0 \tag{21b}$$

$$z_i(t_0) = -\varphi_0 + \bar{\varphi}_{0,i} \tag{21c}$$

where[2] $R = 1$ and $RC_2 v_{C_{2,i}}(t_0) = \bar{\varphi}_{0,i}$. Finally, it is considered a uniform space–invariant weak coupling among the MOCs, i.e., $d_{ik} = d$ for all $i = 1, \ldots, 4$. As a consequence the dynamics of the whole NMOC takes place on the $3N$–dimensional zero–manifold $\mathcal{M}(\mathbf{0})$ and the same periodic/chaotic attractors and bifurcations occurring in locally–connected networks of Chua's circuits can be observed.

Remark 4: Following the approach presented in this section, a comprehensive numerical study can be carried out to make clear the influence of the initial conditions and coupling strength in the synchronization phenomena. Some preliminary results confirm the presence of the co-existing chaotic attractors reported in the literature (see in particular [26], [27]). A systematic analysis can be also extended to networks (e.g., bi–dimensional arrays) of memristor–based Chua's circuit with complex topology.

For the sake of completeness a brief summary of the nonlinear dynamics in cellular nonlinear networks of Chua's circuits [31] is described by the following scenario:

- for the single uncoupled Chua's circuit (or equivalently for the uncoupled MOC on $\mathcal{M}(0)$) with

  $$\alpha = 8, \beta = 15$$

  there are:
  - two stable asymmetric limit cycles A^+ and A^- surrounding the unstable equilibria $(+1.5, 0, -1.5)$ and $(-1.5, 0, +1.5)$, respectively
  - one stable symmetric limit cycle S^s surrounding the unstable equilibrium point $(0, 0, 0)$
  - one unstable symmetric limit cycle S^u
- for a network composed by an arbitrary number (N) of oscillatory Chua's circuits and small coupling d it is derived that (see [31, p. 953]):
  a) there are 2^N stable asymmetric limit cycles with all the phase shifts equal to π;
  b) the other $2^N \times (2^{N-1} - 1)$ asymmetric limit cycles are unstable
  c) there is only one stable symmetric limit cycle with all the phase shifts equal to zero
  d) the other $(2^N - 1)$ symmetric limit cycles are unstable.

The cases a) and c), referred to as phase–locking in oscillatory arrays, are reported in the next subsection, whereas the final subsection shows how the four MOCs array splits into periodic and chaotic clusters.

1) Phase–locking in oscillatory NMOCs: Let us focus on the simple array made of four MOCs ($N = 4$) with uniform space–invariant weak coupling $d = 0.05$ and the ICs given in (21) with $\varphi_0 = 0$, $\bar{\varphi}_{0,1} = 10$ and $\bar{\varphi}_{0,2} = \bar{\varphi}_{0,3} = \bar{\varphi}_{0,4} - 10$. It follows that $X_{c_0} = 0$, $x_i(t_0) = 0$ and $y_i(t_0) = 0$ for all $i = 1, \ldots, 4$, whereas $-z_1(t_0) = z_2(t_0) = z_3(t_0) = z_4(t_0) = 10$. The analysis on synchronization manifolds reported before

[2]See also the normalization values in [29, Table I].

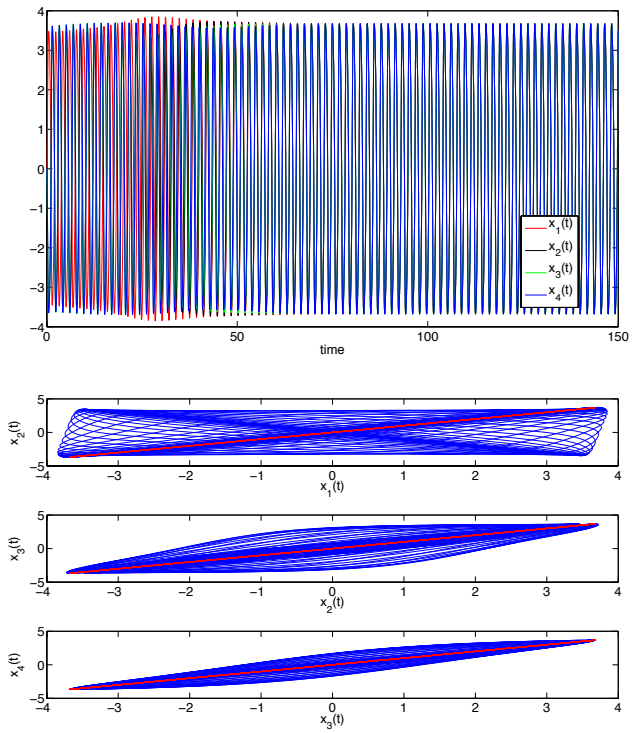

Figure 8: In–phase synchronization among the four MOCs with $d = 0.05$. Waveforms over the time period $[0, 200]$ are shown in the upper part, whereas the phase shifts equal to zero (among the variables $x_i(t)$ for $t \to \infty$) are represented by the red curves in the bottom part of the figure.

permits to conclude that for each MOC the parameter $Q_0 = Q(\mathbf{w}(t_0)) = 0$ and then $\mathbf{Q}_0 = 0$ for the NMOCs described by (16). As a consequence, the nonlinear dynamics of the NMOCs takes place on the manifold $\mathcal{M}_c(\mathbf{0})$ for $t \geq t_0$. In addition, it is apparent that the necessary condition for CS (in–phase synchronization), i.e., $X_{c_{0,i}}$ are equal for all i (cf. (18)), is satisfied. The numerical simulation shown in Fig. 8 confirms the analysis and the scenario reported in c), that is each MOC oscillates according to the symmetric limit cycle (only the variables $x_i(t)$ are reported in Fig. 8). In particular, Fig. 9 presents the waveforms $x_i(t)$ over the time intervals $[0, 25]$ and $[60, 100]$. It is readily derived that, after a transient lasting almost until $t = 60$, an in–phase oscillatory synchronized state emerges due to the weak coupling.

ICs can be changed in such a way that each uncoupled MOC would evolve on an asymmetric limit cycle. In particular the ICs in (21) with $\varphi_0 = 0$, $\bar{\varphi}_{0,1} = 1.1$ and $\bar{\varphi}_{0,2} = \bar{\varphi}_{0,3} = \bar{\varphi}_{0,4} = -1$ have been used (all the other parameters are the same as in the previous case) in the numerical simulation reported in Fig. 10. In such a case, referred to as scenario a) in the summary above, the weak coupling $d = 0.005$ gives rise to a global periodic oscillation in the NMOCs such that there exist π phase shifts among the asymmetric limit cycles of each MOC (note the oscillations of $x_i(t)$, for $i = 1, \ldots, 4$, around -1.5). Such anti–phase synchronized state is shown in the bottom part of Fig. 10 over a time interval $[450, 500]$,

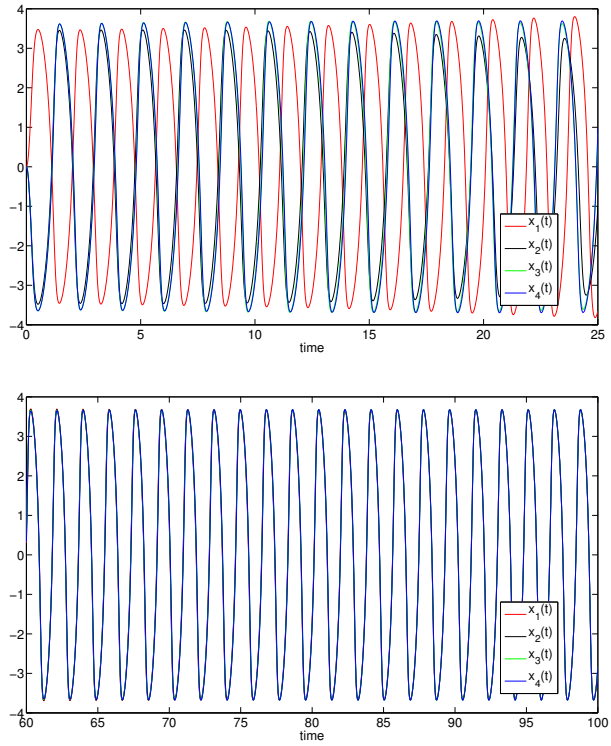

Figure 9: Zoom of the waveforms in Fig. 8 over time intervals $[0, 25]$ (upper part) and $[60, 100]$ (bottom part).

whereas the middle part of Fig. 10 presents the initial transient for $t \in [0, 50]$.

2) Periodic and chaotic clusters in NMOCs: Let us keep ICs as in the previous case (i.e., $\varphi_0 = 0$, $\bar{\varphi}_{0,1} = 1.1$ and $\bar{\varphi}_{0,2} = \bar{\varphi}_{0,3} = \bar{\varphi}_{0,4} = -1$), but $\alpha = 8$ changes over to $\alpha = 9.5$, thus each uncoupled MOC exhibits on the zero–manifold $\mathcal{M}(0)$ a double–scroll chaotic attractor (see Fig. 3 in section II-A). In such a case the change of the parameter α induces a (standard) bifurcation and the complex dynamic scenario is reported in Fig. 11 and Fig. 12 for $d = 0.005$ and Fig. 13 for $d = 0.05$. It is apparent from Fig. 12 that when $d = 0.05$ the whole NMOCs exhibit a chaotic attractors such that the external 1^{st} and 4^{th} MOCs have a periodic synchronized behavior whereas the internal 2^{nd} and 3^{rd} MOCs are chaotic. If the coupling strength d is reduced to 0.005 the whole NMOCs present a chaotic behavior (see Fig. 13).
An extensive numerical analysis has revealed that a wide range of complex dynamical phenomena and bifurcations (standard and without parameters) occur on the zero–manifold of such NMOCs. The invariant manifold analysis presented in Sections II and IV permits to control the manifolds, on which the nonlinear dynamics takes place, via a suitable choice of ICs. Additional results are not included in this manuscript for the lack of space and will be reported in a further publication.

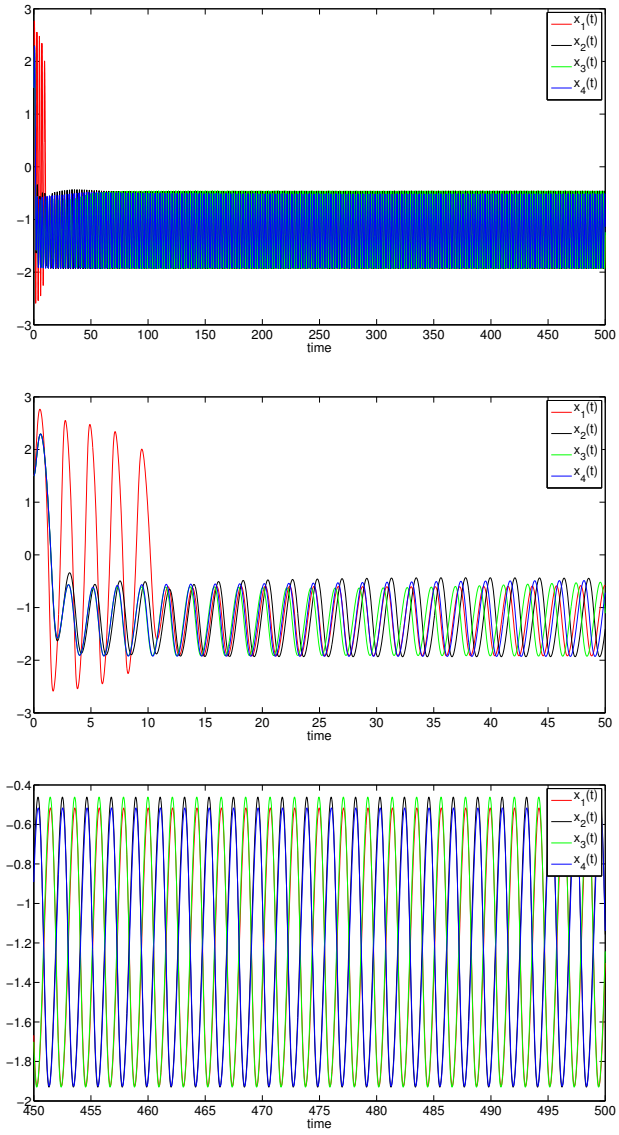

Figure 10: Anti–phase synchronized state in the NMOCs such that there exists a π phase shifts among the periodic oscillation of each MOC. The middle part is the initial transient for $t \in [0, 50]$. In the bottom part it is apparent the π phase shifts among $x_i(t)$ $(i = 1, \ldots, 4)$ over the time interval $[450, 500]$.

V. Conclusion

The manuscript has analyzed complex dynamics, bifurcations, and synchronization phenomena in 1D arrays of diffusively–coupled MOCs. The chief outcome is the description of NMOCs' nonlinear dynamics via an order–reduced dynamical circuits, namely, the state space in the (v, i)–domain has been decomposed in invariant manifolds where NMOCs obey a reduced–order dynamics, depending on the manifold, that is explicitly known in the (φ, q)–domain. In particular, ICs for the state variables in the (v, i)–domain appear as constant inputs in the vector field defining the dynamics in the (φ, q)–domain on each manifold (see the terms $X_{c_{0,i}}$ in the SEs (16) of NMOCs in the (φ, q)–domain). An additional key contribution in the paper is the explicit knowledge of $X_{c_{0,i}}$, which is demonstrated to be crucial for addressing synchronization of NMOCs. Indeed, in order to have complete synchronization it is needed that all $X_{c_{0,i}}$ are the same, which

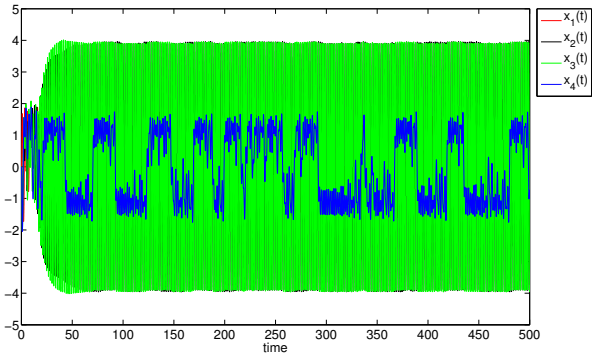

Figure 11: Chaotic behavior in the NMOCs with $d = 0.05$.

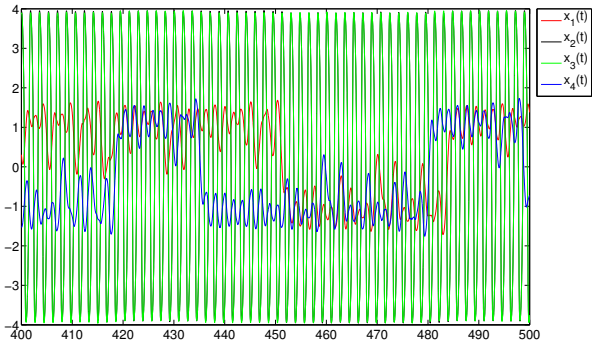

Figure 12: Zoom of the waveforms in Fig. 11.

can be guaranteed by choosing uniformly distributed ICs for memristor fluxes in the uncoupled MOCs. We stress that this necessary condition for synchronization of NMOCs is clearly identifiable via FCAM in the (φ, q)–domain, but it would to be very difficult to identify by a standard analysis of NMOCs in the (v, i)–domain or a daunting task by means of numerical approach. In addition to complete synchronization, the study has also focused on other types of synchronization, such as anti–phase synchronization between limit cycles, and complex chaotic behavior in NMOCs.

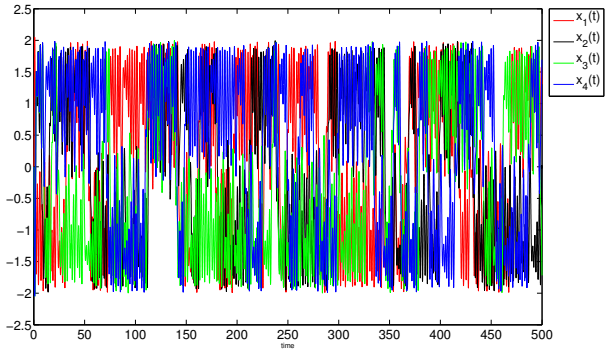

Figure 13: Chaotic behavior in the NMOCs with $d = 0.005$.

REFERENCES

[1] L. O. Chua (Ed.), "Special issue on nonlinear waves, patterns and spatio-temporal chaos in dynamic arrays," *IEEE Trans. Circuits Syst. I, Fundam. Theory Appl.*, vol. 42, no. 10, pp. 557–823, Oct. 1995.

[2] L. O. Chua, "Memristor-The missing circuit element," *IEEE Trans. Circuit Theory*, vol. 18, no. 5, pp. 507–519, 1971.

[3] S. Kumar, J. P. Strachan, and R. S. Williams, "Chaotic dynamics in nanoscale NbO2 Mott memristors for analogue computing." *Nature*, 2017.

[4] A. Pikovsky, M. Rosenblum, and J. Kurths, *Synchronization: a universal concept in nonlinear sciences*. Cambridge university press, 2003, vol. 12.

[5] A.-L. Barabási, "Linked: The new science of networks," 2003.

[6] G. V. Osipov and V. D. Shalfeev, "The evolution of spatio-temporal disorder in a chain of unidirectionally-coupled Chua's circuits," *IEEE Trans. Circ. Syst. I: Fund. Theory Appl.*, vol. 42, no. 10, pp. 687–692, 1995.

[7] M. J. Ogorzalek, Z. Galias, A. M. Dabrowski, and W. R. Dabrowski, "Chaotic waves and spatio-temporal patterns in large arrays of doubly-coupled Chua's circuits," *IEEE Trans. Circ. Syst. I: Fund. Theory Appl.*, vol. 42, no. 10, pp. 706–714, 1995.

[8] F. Kavaslar and C. Guzelis, "A computer-assisted investigation of a 2-D array of Chua's circuits," *IEEE Trans. Circ. Syst. I: Fund. Theory Appl.*, vol. 42, no. 10, pp. 721–735, 1995.

[9] E. Sánchez, M. A. Matías, and V. Pérez-Muñuzuri, "Chaotic synchronization in small assemblies of driven Chua's circuits," *IEEE Trans. Circ. Syst. I: Fund. Theory Appl.*, vol. 47, no. 5, pp. 644–654, 2000.

[10] M. de Magistris, M. di Bernardo, E. Di Tucci, and S. Manfredi, "Synchronization of networks of non-identical Chua's circuits: Analysis and experiments," *IEEE Trans. Circ. Syst. I: Reg. Papers*, vol. 59, no. 5, pp. 1029–1041, 2012.

[11] A. Bogojeska, M. Mirchev, I. Mishkovski, and L. Kocarev, "Synchronization and consensus in state-dependent networks," *IEEE Trans. Circ. Syst. I: Reg. Papers*, vol. 61, no. 2, pp. 522–529, 2014.

[12] H. Liu, M. Cao, and C. W. Wu, "Coupling strength allocation for synchronization in complex networks using spectral graph theory," *IEEE Trans. Circ. Syst. I: Reg. Papers*, vol. 61, no. 5, pp. 1520–1530, 2014.

[13] W. K. Wong, W. Zhang, Y. Tang, and X. Wu, "Stochastic synchronization of complex networks with mixed impulses," *IEEE Trans. Circ. Syst. I: Reg. Papers*, vol. 60, no. 10, pp. 2657–2667, 2013.

[14] D. Kim, M. Jin, and P. H. Chang, "Control and synchronization of the generalized Lorenz system with mismatched uncertainties using backstepping technique and time-delay estimation," *Int. J. Circuit Theory Appl.*, 2017, DOI: 10.1002/cta.2353.

[15] L. S. Smith, "Neuromorphic systems: past, present and future," *Adv. in Exp. Med. and Bio.*, vol. 657, pp. 167–182, 2010.

[16] L. Chua, "Everything you wish to know about memristors but are afraid to ask," *Radioengineering*, vol. 24, no. 2, pp. 319–368, 2015.

[17] A. Ascoli, V. Lanza, F. Corinto, and R. Tetzlaff, "Synchronization conditions in simple memristor neural networks," *Journal of the Franklin Institute*, vol. 352, no. 8, pp. 3196–3220, 2015.

[18] V. Erokhin, T. Berzina, P. Camorani, A. Smerieri, D. Vavoulis, J. Feng, and M. P. Fontana, "Material memristive device circuits with synaptic plasticity: learning and memory," *BioNanoScience*, vol. 1, no. 1-2, pp. 24–30, 2011.

[19] Z. Wang, S. Ambrogio, S. Balatti, and D. Ielmini, "A 2-transistor/1-resistor artificial synapse capable of communication and stochastic learning in neuromorphic systems," *Frontiers in neuroscience*, vol. 8, 2014.

[20] L. V. Gambuzza, A. Buscarino, L. Fortuna, and M. Frasca, "Memristor-based adaptive coupling for consensus and synchronization," *IEEE Trans. Circuits Syst. I: Reg. Papers*, vol. 62, no. 4, pp. 1175–1184, April 2015.

[21] ——, "Memristor-based adaptive coupling for consensus and synchronization," *IEEE Trans. Circ. Syst. I: Reg. Papers*, vol. 62, no. 4, pp. 1175–1184, 2015.

[22] E. Bilotta, F. Chiaravalloti, and P. Pantano, "Spontaneous synchronization in two mutually coupled memristor-based Chuas circuits: Numerical investigations," *Math. Problems in Engineering*, vol. 2014, 2014.

[23] ——, "Synchronization and waves in a ring of diffusively coupled memristor-based Chuas circuits," *Acta applicandae mathematicae*, vol. 132, no. 1, pp. 83–94, 2014.

[24] V.-T. Pham, S. Vaidyanathan, C. Volos, S. Jafari, N. Kuznetsov, and T. Hoang, "A novel memristive time-delay chaotic system without equilibrium points," *Eur. Phys. J.: Spec. Topics*, vol. 225, no. 1, pp. 127–136, 2016.

[25] J. Ma, F. Wu, G. Ren, and J. Tang, "A class of initials-dependent dynamical systems," *Appl. Math. Comput.*, vol. 298, pp. 65–76, 2017.

[26] Q. Xu, Y. Lin, B. Bao, and M. Chen, "Multiple attractors in a non-ideal active voltage-controlled memristor based Chua's circuit," *Chaos, Solitons & Fractals*, vol. 83, pp. 186–200, 2016.

[27] B. Bao, T. Jiang, G. Wang, P. Jin, H. Bao, and M. Chen, "Two-memristor-based Chua's hyperchaotic circuit with plane equilibrium and its extreme multistability," *Nonlinear Dynamics*, pp. 1–15, 2017.

[28] F. Corinto and M. Forti, "Memristor circuits: Flux–charge analysis method," *IEEE Trans. Circuits Syst. I, Reg. Papers*, vol. 63, no. 11, pp. 1997–2009, Nov. 2016, DOI: 10.1109/TCSI.2016.2590948.

[29] ——, "Memristor circuits: Bifurcations without parameters," *IEEE Trans. Circuits Syst. I, Reg. Papers*, vol. 64, pp. 1540–1551, 2017, DOI: 10.1109/TCSI.2016.2642112.

[30] ——, "Memristor circuits: Pulse programming via invariant manifolds," *IEEE Trans. Circuits Syst. I, Reg. Papers*, 2017, in press, DOI: 10.1109/TCSI.2017.2740999.

[31] M. Gilli, F. Corinto, and P. Checco, "Periodic oscillations and bifurcations in cellular nonlinear networks," *IEEE Trans. Circ. Syst. I: Reg. Papers*, vol. 51, no. 5, pp. 948–962, 2004.

[32] W. Lu and T. Chen, "New approach to synchronization analysis of linearly coupled ordinary differential systems," *Physica D: Nonlinear Phenomena*, vol. 213, no. 2, pp. 214–230, 2006.

[33] C. W. Wu and L. O. Chua, "Synchronization in an array of linearly coupled dynamical systems," *IEEE Trans. Circuits Syst. I: Fund. Theory Appl.*, vol. 42, no. 8, pp. 430–447, 1995.

[34] L. O. Chua, "Global unfolding of Chua's circuit," *IEICE Trans. Fundamentals*, vol. E76-A, no. 5, pp. 948–962, May 1993.

[35] M. Itoh and L. O. Chua, "Memristor oscillators," *Int. J. Bifurc. Chaos*, vol. 18, no. 11, pp. 3183–3206, 2008.

[36] B.-C. Bao, Q. Xu, H. Bao, and M. Chen, "Extreme multistability in a memristive circuit," *Electronics Letters*, vol. 52, no. 12, pp. 1008–1010, 2016.

[37] B. Bao, Z. Ma, J. Xu, Z. Liu, and Q. Xu, "A simple memristor chaotic circuit with complex dynamics," *Int. J. Bifurc. Chaos*, vol. 21, no. 9, pp. 2629–2645, 2011.

[38] M. E. Yalcin, "Dynamic behavior of 1-D array of the memristively-coupled Chua's circuits," in *Electrical and Electronics Engineering (ELECO), 2013 8th International Conference on*. IEEE, 2013, pp. 13–16.

[39] F. Corinto and M. Forti, "Nonlinear dynamics of memristor oscillators via the flux-charge analysis method," in *Proc. ISCAS 2017, IEEE Int. Symp. on Circuits and Systems*, Baltimora, MD, May 28-31, 2017, pp. 2739–2742.

[40] L. Ponta, V. Lanza, M. Bonnin, and F. Corinto, "Emerging dynamics in neuronal networks of diffusively coupled hard oscillators," *Neural Networks*, vol. 24, no. 5, pp. 466–475, 2011.

[41] V. Lanza, L. Ponta, M. Bonnin, and F. Corinto, "Multiple attractors and bifurcations in hard oscillators driven by constant inputs," *Int. J. Bifurc. Chaos*, vol. 22, no. 11, p. 1250267, 2012.

[42] R. Genesio and A. Tesi, "Distortion control of chaotic systems: The Chua's circuit," *J. Circuits, Syst., Computers*, vol. 3, no. 01, pp. 151–171, 1993.

[43] F. C. Hoppensteadt and E. M. Izhikevich, *Weakly connected neural networks*. Springer Science & Business Media, 2012, vol. 126.